Astronomy & Astrophysics manuscript no. faraday˙caustics
May 16, 2011

Faraday caustics

Singularities in the Faraday spectrum and their utility as probes of magnetic field properties

M.R. Bell, H. Junklewitz, and T.A. Enßlin

Max Planck Institute for Astrophysics, Karl-Schwarzschild-Str. 1, 85741 Garching, Germany e-mail: mrbell@mpa-garching.mpg.de

Received **???** / Accepted **???**

ABSTRACT

We describe singularities in the distribution of polarized intensity as a function of Faraday depth (i.e. the Faraday spectrum) that arise due to line of sight (LOS) magnetic field reversals. We call these features Faraday caustics due to their similarity to optical caustics. They appear sharply spiked in the Faraday spectrum with a tail that extends to one side. The direction in which the tail extends depends on the way in which the LOS magnetic field reversal occurs (either changing from oncoming to retreating or vice versa). We describe how surfaces of Faraday caustics relate to boundaries between regions where the LOS magnetic field has opposite polarity. Examples from simulations of the polarized synchrotron emission from the Milky Way are provided. We derive the probability or luminosity distribution of Faraday caustics produced in a Gaussian magnetic field distribution as a function of their strength, $\mathcal{F}$, and find that for strong Faraday caustics $P(\mathcal{F}) \propto \mathcal{F}^{-3}$. If fully resolved, this distribution is also shown to depend on the Taylor microscale which relates to the largest scale over which dissipation is important in turbulent flow.

Key words. Polarization - Magnetic Fields - Turbulence

1. Introduction

The availability of broadband receivers in next generation radio telescopes, for example the Expanded Very Large Array (EVLA), the Square Kilometer Array (SKA) and its pathfinder arrays such as the Low-Frequency Array (LOFAR) in the Netherlands, has led to the development of a novel technique for imaging polarized radio emission known as rotation measure (RM) synthesis (Brentjens & de Bruyn 2005). Derived from a technique originally proposed by Burn (1966), RM synthesis allows for the separation of polarized sources along the line of sight (LOS) by reconstructing the distribution of polarized emission as a function of Faraday depth (in the simplest case Faraday depth is equivalent to RM). The technique provides several benefits: sensitivity is improved by combining measurements from hundreds or even thousands of channels over a broad frequency range, the rotation measure of point sources can be measured more accurately and unambiguously, and the intrinsic polarized emission from different sources along a line of sight can be studied independently. Also, because the Faraday depth depends on the integrated LOS magnetic field, RM synthesis promises to be an important tool for studying magnetism.

To date there have been few applications of RM synthesis although interest is rapidly increasing as new radio telescopes are being commissioned. Examples of recent results include studies of the diffuse polarized emission in the Perseus field (de Bruyn & Brentjens 2005; Brentjens 2010) and associated with Abell 2255 (Pizzo et al. 2010), analysis of galactic polarized emission in the WSRT-SINGS survey (Heald et al. 2009), and the detection of a shell of compressed magnetic field surrounding a local HI bubble (Wolleben et al. 2010). RM synthesis will play a critical role in several upcoming polarization surveys, e.g. POSSUM (Gaensler et al. 2010), GMIMS (Wolleben et al. 2009), and future surveys with LOFAR.

The technique of RM synthesis builds on the work of Burn (1966) who showed that the complex polarized intensity, P, as a function of λ^2 is related to the intrinsic complex polarized intensity as a function of Faraday depth, F, by a (nearly) Fourier relationship

$$P(\lambda^2) = \int_{-\infty}^{\infty} F(\phi, \lambda^2) \mathrm{e}^{2i\phi\lambda^2} d\phi. \quad (1)$$

where ϕ, known as the *Faraday depth*, is a measure of the amount of rotation suffered by a linearly polarized wavefront as it passes through a magneto-ionic medium. It is measured in rad m^{-2} and is given by

$$\phi = a_0 \int_0^z n_e(z') B_3(z') dz' \quad (2)$$

where n_e is the number density of thermal electrons, z is distance along the LOS, and $B_3(z')$ is the component of the magnetic field along the LOS. The constant term is $a_0 = e^3/(2\pi m_e^2 c^4) = 0.81$ cm^3 (μG pc)$^{-1}$, where e and m_e are the charge and mass of the electron, respectively.

The quantity $F(\phi, \lambda^2)$ is the intrinsic polarized intensity as a function of Faraday depth. We refer to this quantity as the Faraday spectrum. It is commonly referred to as the Faraday dispersion function following Burn (1966). Though F generically depends on frequency we will assume a separable form, $F(\phi, \lambda^2) = f(\phi)s(\lambda^2)$, allowing for the removal of $s(\lambda^2)$ from the integral in Eq. (1). We will henceforth assume that $P(\lambda^2)$ has been normalized by the spectral dependence such that $P(\lambda^2) = \int F(\phi) \mathrm{e}^{2i\phi\lambda^2} d\phi$.

The Faraday spectrum is a three dimensional description of the polarized emission and may be reconstructed by inverting Eq. (1). In general this is not possible due to our inability to completely sample P for all values of λ^2, but this complication is resolved using the RM synthesis technique of Brentjens & de Bruyn (2005) where the inversion is treated in much the same way as it is in synthesis imaging.

In this paper we are concerned with the properties of the Faraday spectrum of diffuse polarized sources. In particular, we describe singularities in the Faraday spectrum that we call *Faraday caustics*. These arise when the LOS magnetic field changes direction causing a pile-up of emission at a single Faraday depth. They are caustics, much like the well known optical phenomenon, in the sense that they are the result of the non-monotonic mapping of the polarized emissivity from physical depth space into Faraday depth space.

Before we derive a mathematical description of Faraday caustics it is helpful to develop a qualitative understanding of how they might arise. Consider a volume filled with magnetic fields, relativistic and thermal electrons. This volume will produce synchrotron emission and rotate the plane of polarization of a polarized plane wave that propagates through it. In general, the polarized emission from each location along a LOS maps to a different location in Faraday depth space and therefore we expect to find extended structures in RM synthesis observations of such a source. In the event where the magnetic field is changing direction along the LOS, what happens at the point where the field is completely in the plane of the sky? In a region where the LOS field is close to zero the Faraday depth will change very little with physical depth since, according to Eq. (2), the Faraday depth changes linearly with the LOS magnetic field component. Therefore, where $B_3 = 0$ there is no change in Faraday depth. This means that all of the polarized emission which originates from this region will pile up around a single Faraday depth value. This is, qualitatively, the cause of the singularities mentioned earlier.

We have two intentions with this paper. First we wish to inform observers about the existence of these features. We expect them to be ubiquitous in Faraday spectrum cubes of diffuse polarized sources so one must understand Faraday caustics in order to properly understand their data. We describe the basic features of caustics, and provide examples of how they appear in simulations of the Galactic synchrotron emission. Secondly, we investigate how observations of Faraday caustics can be exploited to uncover information about the underlying magnetic field structure and statistical properties. We present a few ideas and examples. This second intention is in line with previous work on the extraction of statistical information of magnetic fields from observables by Spangler (1982, 1983), Eilek (1989a,b), Enßlin & Vogt (2003), Kahniashvili & Vachaspati (2006), Waelkens et al. (2009), Junklewitz & Enßlin (2010), and Oppermann et al. (2010).

In Sect. 2 we derive the properties of Faraday caustics by considering a generic magnetic field near the location where it is aligned in the plane of the sky. We examine the observational manifestation of caustics in Sect. 3, showing examples from simulated synchrotron emission from the plane of the Milky Way. The luminosity function of caustics generated in a Gaussian random magnetic field as a function of their strength is computed in Sect. 4. Finally, in Sect. 5 we present our conclusions.

2. Properties of Faraday caustics

Faraday caustics appear where the magnetic field lies entirely in the plane of the sky, i.e. where $B_z = 0$, in a mixed synchrotron emitting and Faraday rotating medium. In order to characterize the basic features of Faraday caustics in a generic magnetic field configuration we will focus on the region immediately surrounding the location where the LOS component is zero. We label this point z_0, where $B_3(z_0) = 0$, and henceforth for simplicity we will set $z_0 = 0$. Ultimately we want to solve for the Faraday spectrum, $F(\phi)$.

The Faraday spectrum is related to the intrinsic polarized intensity, $P(z)$, by

$$F(\phi) = \int_{-\infty}^{\infty} \delta(\phi - \phi(z)) P(z) dz. \tag{3}$$

The polarized intensity per unit length along z is

$$\begin{aligned} P(z)dz &= p(\alpha) I(z) e^{2i\chi(z)} dz \\ &= a_s(\alpha) \, |B_\perp(z)|^{1+\alpha} \, e^{2i\chi(z)} dz \end{aligned} \tag{4}$$

where a_s contains all of the constant and frequency dependent terms in the expression for the synchrotron emissivity, $I(z)$ (see e.g. Rybicki & Lightman 2004). We have also included the fractional polarization of synchrotron emission, $p(\alpha) = (\alpha + 1)/(\alpha + 5/3)$, within a_s. Here α is the spectral index where $I(\nu) \propto \nu^{-\alpha}$. For convenience we will assume $\alpha = 1$ throughout the remainder of this paper. This assumption is approximately correct for many optically thin synchrotron sources and suits our purpose of providing a basic description. The angle χ is the intrinsic position angle and $B_\perp$ is the magnetic field in the plane of the sky. In order to compute F we require a description of the z dependence of both B_3 and $B_\perp$.

For the sake of generality we will restrict our attention to the region near $z_0 = 0$ and expand the LOS magnetic field around z_0 to first order with respect to z

$$B_3(z) = B_3'(0) z + \ldots \tag{5}$$

where the prime indicates differentiation in z. In this way we will not have to specify a functional form for $B_3(z)$. From Eq. (2) we find

$$\phi(z) - \phi_0 = \frac{a_1 B_3'(0) z^2}{2} \tag{6}$$

where $a_1 = a_0 n_e$ and we assume that $n_e(z)$ is approximately constant over this limited range in z.

At this point we can already start to get a feeling for what happens to $F(\phi)$. The last expression tells us how the polarized emission originating at a given z location maps to ϕ-space; with a linear approximation for the magnetic field ϕ is quadratic in z. The value $\phi(z) = \phi_0$, which occurs when $z = z_0 = 0$, is either a maximum or minimum depending on the sign of $B_3'(0)$ and therefore the Faraday spectrum will extend only to one side or the other of ϕ_0. Also, as $z \to 0$ the change in Faraday depth, $d\phi/dz$, becomes small and the emission over a potentially large range of z values "piles up" over a small range of ϕ values. Therefore we expect that $F(\phi)$ will sharply increase near ϕ_0 and appear as an asymmetric "spike". Since smaller values of $\left|B_3'\right|$ lead to a flatter $\phi(z \sim 0)$, we should expect stronger spikes when the LOS magnetic field changes direction over larger distances.

The magnetic field in the plane of the sky, $B_\perp$, is a vector quantity. We will define it as a complex valued function encoding the position angle within the phase,

$$B_\perp(z) = |B_\perp(z)| \, e^{i\beta(z)} \tag{7}$$

where β is the position angle of the vector in the plane of the sky. For optically thin synchrotron emission $\chi = \beta \pm 90^\circ$ and $\chi' = \beta'$. We also expand $B_\perp$ around z_0 to first order in z

$$B_\perp(z) = |B_\perp(0)|\, e^{i\beta(0)} + \left(|B_\perp|'(0) e^{i\beta(0)} + i\beta'(0)\,|B_\perp(0)|\, e^{i\beta(0)}\right) z + \ldots \quad (8)$$

For illustration we will restrict our attention to the case where $\beta'(0)$ is the important term in the expansion. In this case the sky plane magnetic field is approximated to be

$$B_\perp(z) \approx |B_\perp(0)|\,(1 + i\beta'(0)z)\, e^{i\beta(0)}. \quad (9)$$

We again expand $\chi(z)$ to first order in z

$$\chi(z) = \chi'(0)z = \beta'(0)z \quad (10)$$

where we choose the sky plane coordinates such that $\chi(0) = 0$.

With the magnetic fields specified we can now calculate F. From Eqs. (3), (4), (6), (9) and (10) we find

$$F(\phi) = \int dz \Big[\delta\left(\phi - \phi_0 - \frac{a_1 B_3'(0) z^2}{2}\right) a_s\,|B_\perp(0)|^2 \left(1 + \beta'(0)^2 z^2\right) e^{2i\beta'(0)z}\Big]. \quad (11)$$

In order to perform the z integration we use the following property of the delta function

$$\delta\left(g(x)\right) = \sum_{\overline{x}:g(\overline{x})=0} \frac{\delta\left(x - \overline{x}\right)}{g'(\overline{x})}, \quad (12)$$

where $\overline{x}$ are the roots of $g(x)$, the sum is over all roots, and the prime indicates differentiation with respect to x. The argument of the delta function has two roots, $\overline{z} = \pm\sqrt{2(\phi - \phi_0)/(a_1 B_z'(0))}$. This means that the polarized emission from two values of z will contribute to F at a single value of ϕ. After performing the z integration we find

$$F(\phi) = D\frac{1 + C^2(\phi - \phi_0)}{\sqrt{\phi - \phi_0}} \cos\left(2C\sqrt{\phi - \phi_0}\right) \quad (13)$$

where

$$C = \beta'(0)\sqrt{\frac{2}{a_1 B_3'(0)}} \quad (14)$$

$$D = \frac{2a_s\,|B_\perp(0)|^2}{\sqrt{a_1 B_3'(0)}}. \quad (15)$$

We can write $F(\phi)$ in terms of the unitless parameter $u = 2C\sqrt{\phi - \phi_0}$ (in the case where $\beta'(0) \neq 0$) in which case it has the form

$$F(u) = 2CD\left(1 + \frac{u^2}{4}\right)\frac{\cos(u)}{u}. \quad (16)$$

The relation $F(u)du = F(\phi)d\phi$ can be used to transform between the two formulations. The cosine term results from adding two $P(z)$ values having different position angles and therefore represents a depolarization effect. If $\beta'(0)$ is such that the position angles at $\pm\overline{z}$ are orthogonal to one another, then $F(u) = 0$.

The final form of F, shown in Fig. 1, is as we expect. When u is small, $F(u) \propto 1/u$ which diverges as $u \to 0$ ($\phi \to \phi_0$). As u gets large, $F(u) \propto u\cos(u)$, but at this point the approximation

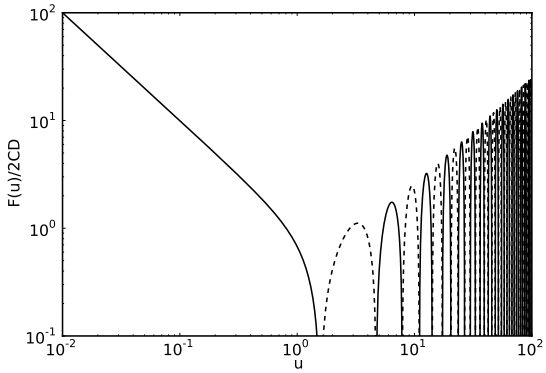

Fig. 1. The dispersion function, $F(u)$, for a caustic. The unitless parameter u is proportional to $\sqrt{\phi}$ and is described in the text. The magnitude of negative values are shown as a dashed line.

that the magnetic field varies linearly with z has broken down. Therefore, our description is restricted to small values of u. This leads to the condition

$$u = 2\beta'(0)\sqrt{\frac{2(\phi - \phi_0)}{a_1 B_3'(0)}} < 1 \quad (17)$$

and so our approximation will be valid when the change in position angle is small, when we are close to ϕ_0, or when the rate of change of the LOS magnetic field is large. As we will see, the latter condition leads to low strength caustic features and since we will primarily be concerned with strong caustics, our description is limited to the regions where the position angle does not change significantly over the limited range in z. Note that the cosine term does not become important until $u > 1$ and the linear approximation is no longer applicable. Therefore, in order to properly describe depolarization effects we need to consider higher order terms in the Taylor expansion of the magnetic field.

Since in many cases caustics will be unresolved in observations (see Sect. 3), we should consider the integrated intensity over the range $\delta\phi$, taken to be approximately the FWHM of the point spread function in ϕ (often called the rotation measure spread function or RMSF). The integrated intensity, $\mathcal{F}$, is

$$\mathcal{F} = \left|\int_{\phi_0}^{\phi_0 + \delta\phi} d\phi\, F(\phi)\right|. \quad (18)$$

After some algebra we find

$$\mathcal{F} = \left|\frac{D}{2C}\sin(u_m)\left(1 + u_m\cot(u_m) + \frac{u_m^2}{2}\right)\right| \quad (19)$$

where $u_m = 2C\sqrt{\delta\phi}$ is the value of u at $\phi = \phi_0 + \delta\phi$. In the limit where $u_m \ll 1$

$$\mathcal{F} = \left|2D\sqrt{\delta\phi}\right| = 4a_s\,|B_\perp(0)|^2\sqrt{\frac{\delta\phi}{a_1 B_3'(0)}}. \quad (20)$$

As expected we find that small values of B_3' lead to strong caustic features. Large $B_\perp$ values will also result in large values of $\mathcal{F}$. However, since the B-field strength is unlikely to deviate significantly from the average and the $1/\sqrt{B_3'}$ term can be arbitrarily large, we argue that strong caustics will mostly be created in regions where B_3' is small. A result of this effect is that large

"spikes" in the Faraday spectrum can result from intrinsically weak emission regions.

Inclusion of higher order expansion terms will not have a significant effect on the basic structure of Faraday caustics described above. In the case of a LOS magnetic field reversal, a caustic will appear as a strongly peaked, asymmetric source in Faraday space regardless of the exact form of the $B_3(z)$ distribution. The higher order terms will affect the shape of the "tail" and have a small effect on the integrated flux over the feature. An exception is the case when the LOS magnetic field reduces to zero but does not change sign. In this case $B_3'(0) = 0$, $B_3(z) \propto z^2$, and $\phi(z) \propto z^3$. The Faraday spectrum will still be strongly peaked at ϕ_0, but the spike will be symmetric in this case with tails extending toward either side of ϕ_0.

It is also worth noting how a caustic appears in λ-space. From Eq. (1) we see that the polarized intensity as a function of λ, $P(\lambda)$, is found by taking the Fourier transform of Eq. (13). Doing so we find

$$P(\lambda) = De^{-2i\lambda^2\phi_0}\frac{(-1-i)\sqrt{\pi}}{2\lambda}. \quad (21)$$

Although this seems to be divergent for $\lambda \to 0$, recall that $P(\lambda)$ has been divided by the a spectral component of the Faraday spectra, $s(\lambda)$. Multiplication by this spectral component ensures that the total physical spectra is finite.

3. Observing Faraday Caustics

Now that we have characterized Faraday caustics (to first order) we can discuss the expected appearance of these features in observations. Since they occur whenever the magnetic field is aligned in the plane of the sky we expect Faraday caustics to be a regularly occurring feature in RM synthesis observations of diffuse polarized fields. Depending on the instrument used and the details of the experimental setup the appearance of Faraday caustics may vary, and as we shall see, may not exhibit the characteristic asymmetry described in the previous section. Nevertheless, Faraday caustics will be present in most observations and so it is important to know what to expect in order to properly interpret Faraday spectra and to learn as much as possible about the underlying magnetic fields.

In lieu of observational data, we make use of the Hammurabi software of Waelkens et al. (2009) to provide examples of Faraday caustics in a realistic Faraday spectrum. This software simulates the Galactic synchrotron emission based on user defined models of the magnetic field, thermal and cosmic ray electron distributions. Hammurabi was first used by Sun et al. (2008) to test Galactic magnetic field models by simulating the resulting polarized foreground emission in the galactic plane. Other examples of its use may be found in Jansson et al. (2009) who compare images of the Galactic synchrotron emission from WMAP5 with simulated emission using several existing Galactic magnetic field models from the literature, in Oppermann et al. (2010) who test the novel LITMUS procedure that probes for the presence of magnetic helicity on simulated sky maps, or in Jaffe et al. (2010) who develop parametrized magnetic field models in the Galactic plane. We have modified Hammurabi to calculate the Faraday spectrum; at each step of the integration along a given LOS we compute the Faraday depth and the intrinsic polarized emission from within the cell. This is stored in a 3-D cube with user defined Faraday depth resolution.

For the examples presented here, Hammurabi was run using the same simulation parameters as Sun et al. (2008) for their

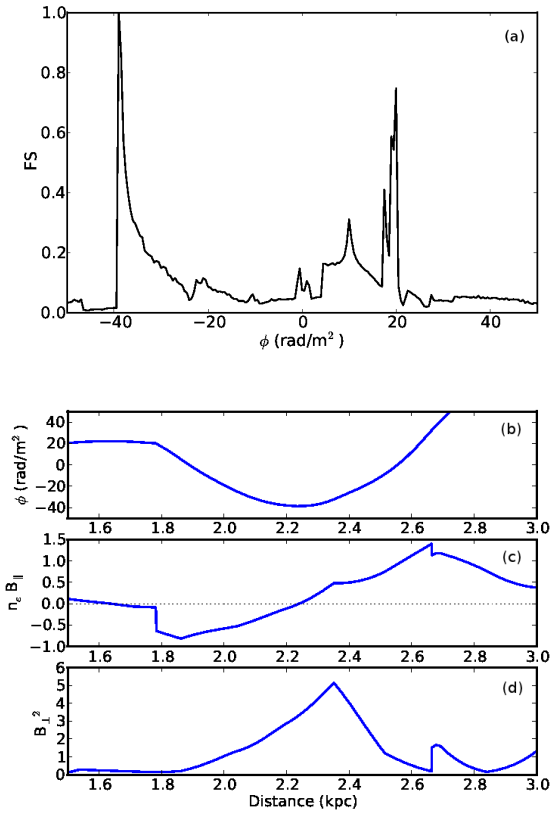

Fig. 2. A Hammurabi simulated Faraday spectrum and the associated Faraday depth and field parameters as a function of physical depth. (a) The Faraday spectrum along the LOS at Galactic coordinates (90°, −15°) in arbitrary units. (b) Faraday depth in rad m^{-2}, (c) The product of the LOS magnetic field and thermal electron density which is proportional to the Faraday depth in code internal units, (d) The perpendicular magnetic field component squared which is proportional to the synchrotron emissivity, again in code internal units.

ASS+RING magnetic field model including a stochastic component (as well as the cosmic ray electron distribution and the thermal electron distribution of Cordes & Lazio (2002)), except at lower angular resolution, and with higher LOS resolution (more integration steps).

We find that the simulated Faraday spectra typically consist of some weak diffuse emission spread over tens of rad m^{-2} as well as many narrow, asymmetric "spikes". In Fig. 2(a) we show a portion of the Faraday spectrum along the LOS at Galactic latitude and longitude (90°, −15°) that provides a clear example of the kind of features discussed in the previous section. Along this LOS we find a prominent caustic feature at $\phi = -39$ rad m^{-2} as well as another small cluster of a few caustic features at $\phi = 19$ rad m^{-2}. The Faraday depth, $\boldsymbol{B}$ and n_e values are shown as a function of LOS distance in Fig. 2(b). The product of n_e and B_3 is related to the Faraday depth, and the quantity $B_\perp^2$ is proportional to the synchrotron emissivity. The caustic feature at −39 rad m^{-2} is associated with the field reversal at $z \sim 2.2$ kpc, where the LOS magnetic field is zero and the synchrotron emissivity peaks. One of the caustics in the cluster around 19 rad m^{-2} is due to the LOS magnetic field zero crossing at $z \sim 1.6$ kpc while others are due to magnetic field structure not shown.

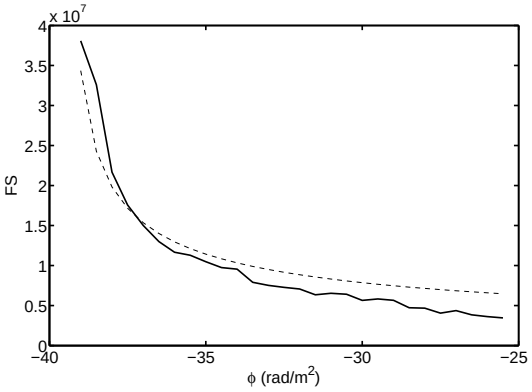

Fig. 3. A portion of the simulated Faraday spectrum from Fig. 2(a). This is compared to the generic form for the Faraday spectrum of a caustic, $F(\phi) \propto 1/\sqrt{\phi}$ (see Eq. (13)), shown as a dashed line.

The major caustic shown in Figure 2(a) at $\phi = -39$ rad m^{-2} exhibits the primary features described in the previous section very clearly. It is strongly spiked, has the characteristic asymmetric shape, and is reasonably well fit by the generic $F(\phi) \propto 1/\sqrt{\phi - \phi_0}$ form as is shown in Fig. 3. The tail extends towards higher values of ϕ as a result of the positive slope of the $B_3(z)$ distribution at $z = 2.2$ kpc.

It should be possible to resolve particularly strong and isolated caustic features such as the one shown here, thereby allowing one to observe the characteristic asymmetry and possibly even to reconstruct the shape of the tail of the spike. The ability to resolve Faraday caustics will not only provide a means of identification, but also information about the magnetic field strength and structure. For instance, the direction of the "tail" of the spike is dictated by the sign of $B_3'(z_0)$. If B_3 changes from positive to negative then the Faraday caustic will be extended in $\phi < \phi_0$. In addition, if one were able to fit the tail to Eq. (13) it would provide a measure of D and therefore of the ratio $B_\perp^2(0)/\sqrt{B_3'(0)}$.

What are the necessary conditions for resolving a Faraday caustic? Brentjens & de Bruyn (2005) give the resolution, $\delta\phi$, and maximum observable scale in Faraday depth space for an RM synthesis experiment as

$$\delta\phi \sim \frac{2\sqrt{3}}{\Delta\lambda^2} \tag{22}$$

$$\text{max. scale} \sim \frac{\pi}{\lambda_{min}^2} \tag{23}$$

where $\Delta\lambda^2$ is the sampled range in λ^2 and λ_{min} is the minimum sampled wavelength. In order to reconstruct the shape of the caustic, the width must be several times $\delta\phi$. Due to their narrow, sharp shape high Faraday depth resolutions will be required in order to resolve Faraday caustics. In order to achieve long "baselines" in λ^2-space an experiment must extend to low frequencies. This will mean that low frequency instruments such as LOFAR will be ideally suited for observing these types of features. Provided that a particular Faraday caustic is strong enough, we also require that the maximum scale is larger than the resolution in order to have a chance of reconstructing its shape. From Eqs. (22) and (23) we find that this condition is satisfied if

$$\frac{\nu_{max}}{\nu_{min}} >\sim 1.5. \tag{24}$$

Consider the high-band LOFAR receivers which operate between 110 and 250 MHz. The FWHM of the main peak of the point spread function in Faraday depth space is $\delta\phi \sim 0.5$ rad/m^2 and the maximum ϕ scale is roughly three times larger.

As an example of what we can expect caustics to look like in real data we can "observe" our simulated Faraday spectra by inverse transforming to λ^2-space, sampling at some set of frequencies, and then transforming back to ϕ-space. Figures 4(a) and 4(b) show the Faraday spectrum of Fig. 2(a) as "observed" using two different frequency ranges. The frequency range used for Fig. 4(a) is 110 to 250 MHz similar to the LOFAR high band antennas. The frequency range used for Fig. 4(b) is 300 to 900 MHz similar to the low frequency portion of the GMIMS survey (Wolleben et al. 2009). We include 512 frequency samples over each range. Most next generation instruments are able to observe using many more frequency channels than this. In each figure we show the Faraday spectrum after deconvolution using our own RMCLEAN software that implements a procedure similar to that described by Heald et al. (2009). The RMCLEAN components are shown in red.

In the "LOFAR" reconstructed spectrum the stronger caustic is reasonably well recovered. The shape of the tail is not exactly as it is in the original spectrum, but the asymmetry is clearly visible. The small cluster of caustics at $\phi \sim 20$ rad/m^2 is resolved showing the three distinct peaks. The same can not be said of the "GMIMS" spectrum. Due to the lower resolution ($\delta\phi \sim 5$ rad/m^2 compared to ~ 0.5 rad/m^2 for the "LOFAR" observation) the individual peaks at $\phi \sim 20$ rad/m^2 are not resolved. The shape of the large caustic is completely lost despite the fact that the tail of the feature extends over 15 rad/m^2 in the original spectrum. No asymmetry is present even in the distribution of CLEAN components.

Having described the appearance of individual caustic features in an observed Faraday spectrum, we now investigate how these will be distributed throughout the 3D Faraday spectral cube. Faraday caustics will be generated at the boundaries of regions having opposite LOS magnetic field polarity. If the magnetic field distribution is sufficiently ordered, this boundary will be a connected and smooth surface in physical space that will map to a similarly connected surface in ϕ-space. Therefore, Faraday caustic surfaces will reflect boundaries between regions of opposite LOS magnetic field polarity.

As mentioned in the previous section, there will be a symmetric variety of caustics that appear as a result of the LOS magnetic field approaching zero tangentially without changing sign. Such features will appear when the boundary between regions of opposite LOS magnetic field polarity is aligned along the LOS, i.e. where a Faraday caustic surface folds over.

In Figs. B.1 and B.2, shown in Appendix B, we show six slices from a Hammurabi simulated Faraday spectral data cube at different Galactic latitudes. The top panel of each slice shows the Faraday spectrum as a function of Galactic longitude and Faraday depth, while the bottom panel shows the LOS magnetic field strength as a function of Galactic longitude and LOS distance. The scale of the magnetic field strength has been compressed to highlight the regions of opposite polarity. White regions indicate a negative LOS magnetic field, black regions a positive field, and the colored sections highlight the boundaries where $B_3 \approx 0$.

In each slice we can see that the smoothly connected boundaries between regions of opposite LOS magnetic field polarity produce connected lines of Faraday caustics in ϕ-space. The caustics can be seen clearly in the Faraday spectra, appearing as sharp, bright lines with faint tails extending to one side.

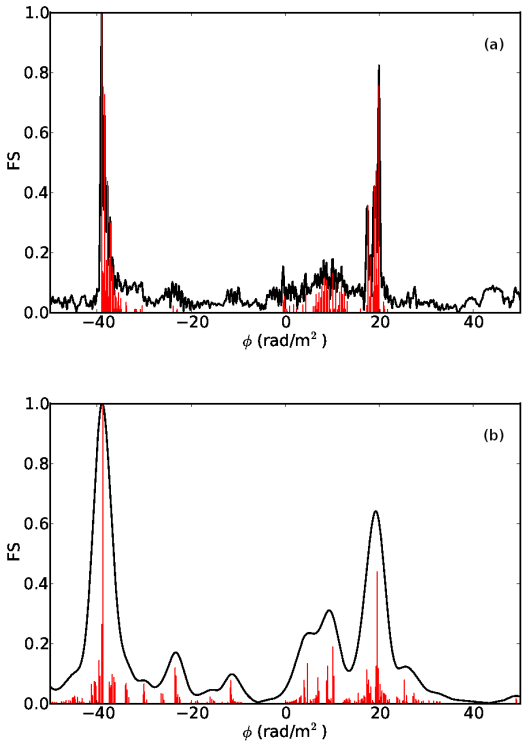

Fig. 4. Mock observations of the Faraday spectrum shown in Fig. 2(a). The spectrum has been observed over two frequency ranges: (a) 110 to 250 MHz, similar to the LOFAR high band antennas and (b) 300 to 900 MHz similar to the low frequency portion of the GMIMS survey. In each figure the Faraday spectrum has been deconvolved using RMCLEAN. The black line represents the restored spectrum while the RMCLEAN components are shown as vertical grey lines (red in the online version).

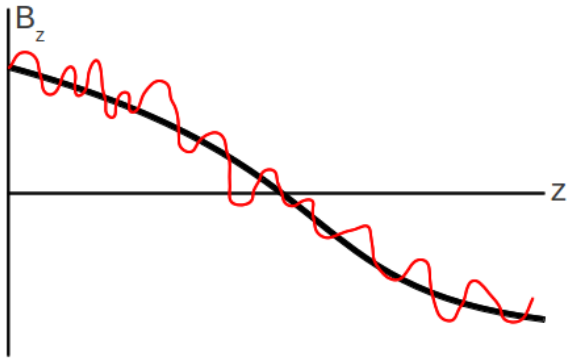

Fig. 5. A diagram illustrating how small scale fluctuation about a larger scale magnetic field variation may split a single Faraday caustic (occurring at the zero crossings) into several smaller caustics. An observation will not be sensitive to fluctuations below a given scale length that depends on the resolution of the experiment.

Watching how the lines move from frame to frame we can get a sense of how the caustics are distributed in 3D, and create a surface of bright polarized emission. In Figure B.1, at Galactic latitude $-117.6°$, a continuous line of caustic features extends from Galactic longitude 15° and $\phi \approx -5$ to Galactic longitude 60° and $\phi \approx 0$. This surface reflects the $B_3 = 0$ boundary at $z \approx 0.2$ kpc. This continuous line remains dominant until frame c, where the polarized emission has shifted to $\phi = 0$ rad/m^2. At this point a second $B_3 = 0$ surface where the LOS magnetic field changes from negative to positive is forming between 4 and 6 kpc. The $B_3 = 0$ surface between longitudes -15° and 15° and at $z \sim 0.6$ kpc produces the line of Faraday caustics between $\phi \sim 0$ and 5 rad/m^2.

In Figure B.2 the rightmost $B_3 = 0$ surface produces the dominant lines of Faraday caustics extending into positive ϕ values in the Faraday spectra. The Faraday caustic surface associated with the leftmost $B_3 = 0$ surface is now at $\phi = 0$ rad/m^2. Note that the tails of the caustic spikes extend between the two surfaces since the LOS magnetic field changes from negative to positive causing one set of caustics, and from positive to negative for the other.

Depending on the smoothness of the magnetic field variation, and the resolution of a given experiment, the caustic surface may consist of a single, well defined peak or a tight cluster of smaller spikes. Consider the LOS magnetic field sketched in Fig. 5. Here the black line represents a large-scale variation of the magnetic field while the grey curve (red in the online version) represents small-scale fluctuations about this distribution. For a smooth variation such as that represented by the black line, a single Faraday caustic will be present. In the case of the red curve three caustics will be created close to one another in ϕ-space. The limited resolution of a given experiment acts to effectively smooth the magnetic field distribution by setting a minimum length scale below which the experiment is not sensitive to variations. This is because the $\delta\phi$ resolution implies a finite resolution in z-space as well. So we expect Faraday caustic surfaces to be either sharp, smoothly connected features in the Faraday spectra or a more "fuzzy" boundary depending on the scale of fluctuation of the magnetic field and the resolution, $\delta\phi$.

4. Distribution of Faraday caustics in a Gaussian random magnetic field

We have just shown how Faraday caustics can inform us about the structure of the LOS magnetic field through their shape and 3D distribution. It is variation and turbulence in the magnetic field which leads to caustics; after all there would be no such features in a purely uniform magnetic field. It may be possible to recover information about the statistical properties of the underlying magnetic field in a source by studying the distribution of caustics within its Faraday spectrum. In this section we investigate the production of Faraday caustics by a Gaussian random magnetic field and calculate the probability distribution, or luminosity function, of "spikes" as a function of their strength.

We assume that the magnetic field distribution is a Gaussian random field with given covariance matrix M. For a Gaussian random field, the covariance matrix is also equal to the correlation tensor. The translationally invariant magnetic correlation

tensor for homogeneous and isotropic magnetic turbulence is

$$\begin{aligned} M_{ij}(r) &= \left\langle B_i(\mathbf{x})B_j(\mathbf{x}+\mathbf{r})\right\rangle \\ M_{ij}(r) &= M_N(r)\delta_{ij} + (M_L(r) - M_N(r))\frac{r_i r_j}{r^2} \\ &\quad + M_H(r)\epsilon_{ijm}r_m \text{ in real space} \\ \hat{M}_{ij}(k) &= \hat{M}_N(k)(\delta_{ij} - \frac{k_i k_j}{k^2}) \\ &\quad - i\epsilon_{ijm}\hat{H}(k)\frac{k_m}{k} \text{ in Fourier space} \end{aligned} \tag{25}$$

(Subramanian 1999, e.g.) where the longitudinal, normal, and helical auto-correlation functions, $M_L(r)$, $M_N(r)$, and $M_H(r)$ respectively, only depend on the distance, not on the direction. Note that $M_N(k)$ can be expressed in terms of the 1D magnetic power spectrum $\epsilon_B(k)$ as

$$\epsilon_B(k) = \frac{k^2 M_N(k)}{8\pi}. \tag{26}$$

The probability to measure an integrated intensity of $\mathcal{F}$ at some location z_0 given that there is a Faraday caustic at z_0 and that the magnetic covariance matrix M is

$$P(\mathcal{F}|\text{caustic}, M) = \frac{P(\mathcal{F}, \text{caustic}|M)}{P(\text{caustic}|M)}. \tag{27}$$

The denominator, $P(\text{caustic}|M)$, is fairly straightforward to compute

$$P(\text{caustic}|M) = \int \mathcal{D}B\ \delta(B_3(z))\ \mathcal{G}(B, M). \tag{28}$$

Here $\mathcal{D}B$ indicates a phase space integral over all possible B-field configurations. Also $\mathcal{G}(\boldsymbol{B}, M)$, a Gaussian probability density function over this phase space, is

$$\mathcal{G}(B, M) = \frac{1}{\sqrt{|2\pi M|}} e^{-\frac{1}{2}B^\dagger M^{-1} B}, \tag{29}$$

where vertical bars indicate that the determinant is to be taken. Here, the notation $A^\dagger B$ implies a multidimensional scalar product such that

$$A^\dagger B = \sum_i \int dx^3\ A_i^*(x) B_i(x). \tag{30}$$

The sum is over the field components and the integral is over physical space.

We find that the probability for a caustic to occur (i.e. $B_3(z_0) = 0$) is

$$P(\text{caustic}|M) = \sqrt{\frac{2\pi}{M_{33}(0)}} \tag{31}$$

where M_{33} is the component of M that describes the two-point correlation between z components of the magnetic field. For the derivations of all results in this section, see Appendix A.

The calculation of the numerator is significantly more involved and as we describe in Appendix A, Eq. (27) can only be computed analytically in the limit where $\mathcal{F}$ is large (we will define this more clearly below). In this limit we obtain the result

$$P(\mathcal{F}|\text{caustic}, M) = \frac{448 a_s^2 \delta\phi^3}{a_1^2} \frac{M_N^2(0)}{\sqrt{2\pi\left|M_{33}''(0)\right|}} \frac{1}{\mathcal{F}^3}. \tag{32}$$

We find that, over a limited range in $\mathcal{F}$, the distribution of the integrated flux of caustics will be proportional to $\mathcal{F}^{-3}$. Note that this indicates that the number of spikes per logarithmic interval of $\mathcal{F}$ is $\propto \mathcal{F}^{-2}$ and thus the Faraday caustic flux per logarithmic interval of $\mathcal{F}$ goes as $\mathcal{F}^{-1}$ which is finite as $\mathcal{F} \to \infty$.

The fore-factors in Eq. (32) depend on the properties of the magnetic field and of the turbulent flow of the fluid in which they are situated. The term $M_N(0)$ is simply the total magnetic energy density. We also introduce the *Taylor microscale*, l_T, which is defined by

$$\left.\frac{d^2 C(z)}{dz^2}\right|_{z=0} = \frac{2}{l_T^2} \tag{33}$$

(see e.g. Tennekes & Lumley 1972, sec. 6.4) where $C(z)$ is the covariance in z normalized to unity at $z = 0$. This length scale represents the largest scale at which dissipation is important in a turbulent flow. The second derivative of the LOS component of the magnetic correlation tensor, $M_{33}''(0)$, is proportional to ϵ_B/l_T^2. We can therefore rewrite Eq. (32) as

$$P(\mathcal{F}|\text{caustic}, M) = \frac{448 a_s^2 \delta\phi^3}{a_1^2} \frac{\epsilon_B^{3/2} l_T}{\sqrt{4\pi}} \frac{1}{\mathcal{F}^3}, \tag{34}$$

where ϵ_B is the total magnetic energy density.

By measuring the distribution of the number of Faraday caustics per integrated flux $\mathcal{F}$ in the $\mathcal{F}^{-3}$ regime, one is then in principle able to measure the Taylor microscale in a turbulent medium. Fletcher & Shukurov (2007) show that this length scale is also measurable by observing the mean separation between so called "depolarization canals," which are lines of zero polarized intensity in a diffuse polarized field. These canals have been observed in maps of the diffuse polarized galactic emission by, e.g. Uyaniker et al. (1998), Haverkorn et al. (2000), Gaensler et al. (2001), and Reich et al. (2004). Observations of depolarization canals and Faraday caustics in tandem may be a powerful tool for studying the turbulent properties in, e.g. the ISM.

A rather important caveat, applicable to both Faraday caustics and depolarization canals, is that without sufficiently high resolution one will not be able to measure this scale. In the case of caustics, as discussed in the previous section, the effect of small scale fluctuations is to split a single Faraday caustic into a tight bundle of spikes. Without enough resolution, an observer may simply count such a bundle as one large spike. This has the effect of altering the normalization of the number distribution of caustics in $\mathcal{F}$ which would lead to an incorrect measurement of l_T. In principle the same effect applies to depolarization canals, where what appears to be a single canal of net zero polarized intensity may in fact be a fine network of such canals. The effect of finite resolution is to smooth the quantity being measured, e.g. the LOS magnetic field distribution in the case of Faraday caustics, thereby throwing away information at scales smaller than this. If the Taylor microscale is smaller than this smoothing scale, then it will not be measurable. We suspect that this may be the case in the example presented by Fletcher & Shukurov (2007) where the Taylor scale of the Milky Way is measured to be much larger than expected.

This result given in Eq. (34) will be valid for strong spikes, i.e. when $B_3'(0)$ is small, but we expect that below some value of $\mathcal{F} = \mathcal{F}_{low}$ the distribution will flatten. This is required in order for the integral of $P(\mathcal{F}|\text{caustic}, M)$ to be finite for $\mathcal{F} \to 0$, but we can also see that this will be the case by considering the approximation applied during our derivation.

In the process of the calculation, so that we may compute the probability analytically, we neglect an exponential term in

Eq. (A.9). This term is $\exp(-\mu K B_\perp^4/\mathcal{F})$, where $K = 16 a_s^2 \delta\phi/a_1$. This is, of course, only valid if the argument of the exponent is much less than one. The approximation breaks down when this term approaches unity, which leads to the following condition for $\mathcal{F}_{low}$

$$\mathcal{F}_{low} \approx \left\langle B_\perp^2 \right\rangle \sqrt{\frac{K}{\left\langle B_3' \right\rangle}} \tag{35}$$

$$\approx K^{\frac{1}{2}} \epsilon_B^{\frac{3}{4}} \lambda_B^{-\frac{1}{2}} \tag{36}$$

where

$$\epsilon_B = \int_0^\infty dk \epsilon_B(k) \tag{37}$$

is the average magnetic energy density, $\epsilon_B(k)$ is the 1D magnetic power spectrum, and

$$\lambda_B = \frac{\pi \int_0^\infty dk \epsilon_B(k)/k}{\int_0^\infty dk \epsilon_B(k)} \tag{38}$$

is the magnetic correlation length.

If we wish to evaluate Eq. (A.9) in all regimes we can no longer neglect this term. While the full calculation is beyond the scope of this paper, we can consider what effects the inclusion of this term might have on the result. To proceed without approximations we would use a pertubative expansion in Feynman diagrams as is used in quantum field theory. The first term in such an expansion would be negative and $\propto \mathcal{F}^{-2}$, the second positive and $\propto \mathcal{F}^{-1}$ and so on. The result is a turnover of the spectrum near $\mathcal{F}_{low}$.

We also expect that the distribution will steepen at larger values of $\mathcal{F}$ due to depolarization. As discussed above, large values of $\mathcal{F}$ imply that the LOS magnetic field changes over long distances. As this happens it is increasingly more likely that the position angle of the polarized emission at the values of z which contribute to the polarized intensity at a single value of ϕ will be uncorrelated resulting in a reduction in the integrated intensity due to depolarization. This reduces the number of caustic features at high values of $\mathcal{F}$.

In order to investigate the conditions for a steepening of the probability distribution of caustics, we consider the correlation of the sky plane magnetic field as a function of LOS distance.

$$\mathcal{R} = \frac{\langle B_\perp(\overline{z}) B_\perp(-\overline{z}) \rangle}{\left\langle B_\perp^2(0) \right\rangle} \tag{39}$$

where the average is over all possible field configurations. The procedure for computing these expectation values is similar to that used in Appendix A to compute $P(\mathcal{F}|caustic, M)$ and therefore not included here. The result is

$$\mathcal{R} = \frac{3 M_N(2\overline{z})}{10 M_N(0)} + \frac{7 M_N^2(\overline{z})}{10 M_N^2(0)}. \tag{40}$$

A small value of $\mathcal{R}$ indicates that, on average, the sky plane magnetic fields are uncorrelated. When this is true the luminosity function will be steeper than $\mathcal{F}^{-3}$.

As an example of estimating $\mathcal{F}_{low}$ and $\mathcal{R}$ we will model the magnetic power spectrum as a broken power law

$$\epsilon_B(k) = \epsilon_0 \left(\frac{k}{k_0}\right)^b \left[1 + \left(\frac{k}{k_0}\right)^2\right]^{-\left(\frac{a+b}{2}\right)}. \tag{41}$$

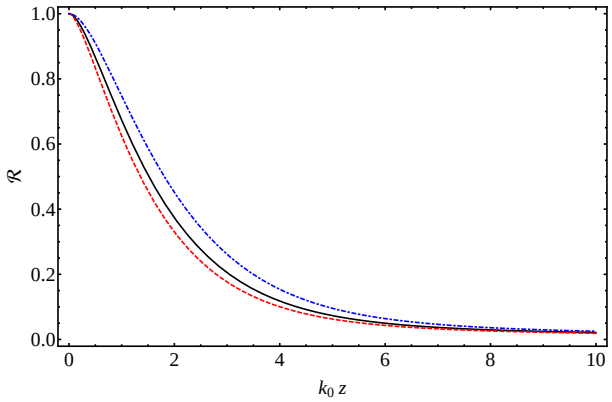

Fig. 6. The normalized correlation of the sky plane magnetic field as a function of $k_0 z$ for a few values of the power law index a. Dashed red $a = 4/3$, solid black $a = 5/3$, dot-dashed blue $a = 7/3$.

For such a power spectrum the luminosity function turns over at

$$\mathcal{F}_{low} = \pi^2 \sqrt{K} \left(\frac{\epsilon_0 k_0^{5/3}}{2}\right)^{\frac{3}{4}} \mathcal{B}\left(\frac{a-1}{2}, \frac{b+1}{2}\right)^{\frac{5}{4}} \mathcal{B}\left(\frac{a}{2}, \frac{b}{2}\right)^{-\frac{1}{2}} \tag{42}$$

where $\mathcal{B}(x)$ is the Beta function.

We can also compute $\mathcal{R}$ since

$$M_N(z) = \int dk \hat{M}_N(k) e^{-ikz} \tag{43}$$

and

$$\hat{M}_N(k) = \frac{8\pi^3 \epsilon_B(k)}{k^2}. \tag{44}$$

The resulting form of $\mathcal{R}(k_0 z)$ is shown for a few representative values of a in Fig. 6. For a Kolmogorov spectrum, $a = 5/3$. In each case, $b = 2$. Note that $\mathcal{R}$ is independent of the parameter ϵ_0.

A calculation of the precise shape of the distribution for low and high values of $\mathcal{F}$ is beyond the scope of this paper. A sketch summarizing the expected shape of the probability distribution, represented as the number of caustics per logarithmic scale of $\mathcal{F}$ as a function of $\log \mathcal{F}$, is shown in Fig. 7. The $\mathcal{F}^{-2}$ region is valid given the assumptions outlined above. At large $\mathcal{F}$ the distribution steepens due to depolarization. At lower values of $\mathcal{F}$ the distribution flattens as higher order effects become more important. We expect that the exact shape of the distribution at low strength will be more strongly dependent on the magnetic field statistics since weak caustic features depend more strongly on $|B_\perp(0)|$. Eventually at low $\mathcal{F}$ the distribution will turn over since the total population of caustics is finite.

In summary, we have calculated the probability density function of caustics having a particular strength in a Gaussian random magnetic field. This result should stand as an example of the type of analysis that is possible and as the simplest reference case for future observations of the luminosity function of Faraday caustics. We caution that the result is limited for several reasons. For one we have assumed an unrealistic magnetic field distribution. This was done for simplicity, but also because if one is not aware of any statistical properties of magnetic field other than the two point correlation, the assumption of a Gaussian field is the most appropriate starting point. Any further knowledge would always be included by expanding around the Gaussian case. While we expect our result in the $\mathcal{F}^{-3}$ regime

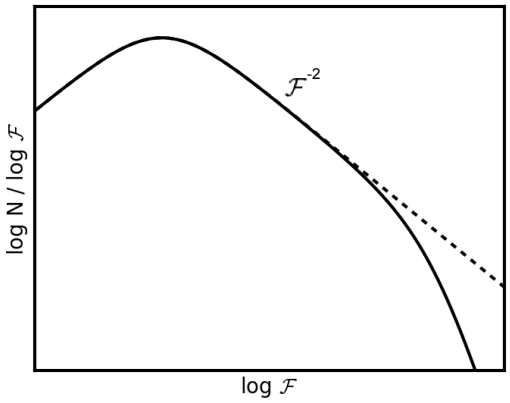

Fig. 7. A sketch of the number distribution of caustic spikes per logarithmic interval of $\mathcal{F}$ showing the limits to the $\mathcal{F}^{-2}$ regime and the rough shape of the distribution beyond these limits. At high values of $\mathcal{F}$ the distribution steepens due to depolarization effects, while at lower $\mathcal{F}$ values the distribution turns over since the total number of caustics is finite. Refer to the text for more details.

to be only weakly dependent on the magnetic field statistics, realistic magnetic field distributions are likely to be significantly non-Gaussian. We have not investigated the degree to which this will effect our results. Secondly, the result in Eq. (34) is only valid over a limited range of $\mathcal{F}$ values. The precise extent of this range is unclear at the moment although we present some estimates. It is possible that the flattening and steepening regimes that we describe are near one another or even overlapping. A more detailed investigation into the flattening regime, for example, would require much more complicated calculations and, because it depends strongly on the magnetic field statistics, a more realistic model.

Lastly, Eq. (34) is truly only valid for very high resolution observations or simulated data. As discussed above, the result will change depending on ϕ-space resolution. In our treatment we simply count the number of zero-point crossings of the LOS magnetic field. In observations, two or more such events in physical space may occur at nearly the same ϕ location and may therefore be counted as a single caustic. This will have the effect of changing the overall normalization of the distribution (the total number of caustics is reduced), however, the $\mathcal{F}^{-3}$ regime should maintain its shape. Analysis of simulations would be helpful in order to investigate the extent of this effect.

5. Discussion and Conclusions

In this paper we have introduced sharp, asymmetric features in the Faraday spectrum of a diffuse polarized source that appear as a result of a change in the direction of the LOS magnetic field. We call these features Faraday caustics. We have derived the form of a Faraday caustic by considering the LOS magnetic field near the point where $B_3 = 0$. The basic properties of a Faraday caustic are:

- They are singularities in the Faraday spectrum and the polarized intensity peaks sharply at the Faraday depth ϕ_0 that maps to the physical depth z_0 where $B_3(z_0) = 0$.
- The Faraday spectrum extends only to one side of the singularity. The direction in which the tail extends depends on the slope of the $B_3(z)$ distribution. If $B_3'(z) > 0$ then the tail extends to $\phi > \phi_0$. The exception is when $B_3(z)$ approaches zero tangentially without changing sign. In this case the caustic is still strongly peaked, but symmetric.
- Strong caustics will predominantly be created when the LOS magnetic field changes over large physical distances i.e. when $B_3'(z_0)$ is small. In this case, the polarized emission from even a relatively weakly emitting region (in physical space) can appear as bright point sources in the Faraday spectrum because the emission over a long LOS distance can pile up over a narrow range of Faraday depths.
- In a 3D Faraday spectral cube Faraday caustics will appear as continuous sheets or surfaces. These surfaces are related to boundaries between regions of opposite LOS magnetic field polarity.
- The effect of small scale fluctuations about larger scale variations will be to split a single large Faraday caustic into a series of smaller, closely packed caustics. Without sufficiently high resolution, this splitting will not be observed. In this way the finite resolution of an experiment acts to smooth the $B_3(z)$ distribution.

We find that important information about the magnetic field distribution can be recovered by observing these features. Reversals of the LOS magnetic field can be identified and if the asymmetry of the Faraday caustics is recovered one will even be able to indicate in which direction the reversal occurs. We have also shown that there may be great value in studying the statistical properties of Faraday caustics. We compute the probability distribution of the polarized intensity of Faraday caustics in a Gaussian random magnetic field. The number of caustics per unit $\mathcal{F}$, which is the integrated intensity of a single caustic, goes as $\mathcal{F}^{-3}$. There is a lower $\mathcal{F}$ limit at which the distribution flattens and turns over, and a high $\mathcal{F}$ limit where the distribution steepens due to depolarization effects. More work is needed to better define these limits, but this should be a fruitful endeavor because we expect that they will depend on the statistical properties of the magnetic field distribution. We show that if one has sufficiently high resolution and measures this distribution in the $\mathcal{F}^{-3}$ regime one can recover the Taylor microscale. This scale is the largest distance over which dissipation is important in a turbulent flow.

It should be noted that caustics may have already been observed. Though we have not analyzed the data directly, the published data from the Perseus field (de Bruyn & Brentjens 2005; Brentjens 2010) contains many point-like features, some of which seem to be connected in what may be the Faraday caustic sheets we discuss above. A re-analysis of these data may provide the first observational evidence of Faraday caustics.

New observational techniques and imaging algorithms may be needed in order to optimally observe Faraday caustics. When investigating the efficacy of a wavelet-based approach to RM synthesis, Frick et al. (2011) note sharp, point-like features in a Faraday spectrum produced by the small scale fluctuations included in their model magnetic field distribution. These features, though not identified as such, are caustics. They show that wavelet-based RM synthesis is effective at separating small and large scale features in the Faraday spectrum and as a result the wavelet-based algorithm outlined in Frick et al. (2010) may be a useful tool for observing Faraday caustics. In addition, matched filter algorithms could be helpful if one wants to more accurately reconstruct the shape of the "tails" which should contain most of the total polarized flux.

Faraday caustics will not be the only source of point-like structure in the Faraday spectrum of a diffuse source. Point sources in Faraday space will also occur as a result of a discrete source along the LOS such as a pulsar or any strong, compact emitter. These discrete sources will also appear as compact sources in the sky plane and will often have associated structure in total intensity making them easy to rule out as caustics. Of course if a caustic is resolved, the asymmetric shape will be an obvious means of identification. In the case of structures more extended in Faraday depth space than the largest measured scale (see Eq. (23)), the extended nature of the source will not be recovered and the edges of the structure will appear to be point-like. In short, confusion with other sources is a possibility but it should not be a big danger.

Acknowledgements. This research was performed in the framework of the DFG Forschergruppe 1254 Magnetisation of Interstellar and Intergalactic Media: The Prospects of Low-Frequency Radio Observations. We acknowledge Rainer Beck, Michiel Brentjens, Andrew Fletcher, Ue-Li Pen, Wolfgang Reich, and Xiaohui Sun for their helpful ideas and insights. We also thank Marco Selig, Helin Weingartner, and Maximilian Uhlig for many useful discussions, and especially Niels Oppermann for his careful reading of our manuscripts. Some of the results in this paper have been derived using the HEALPix package (Górski et al. 2005).

References

Brentjens, M. A. 2010, 1011.0854
Brentjens, M. A. & de Bruyn, A. G. 2005, Astronomy and Astrophysics, 441, 1217
Burn, B. J. 1966, Monthly Notices of the Royal Astronomical Society, 133, 67
Cordes, J. M. & Lazio, T. J. W. 2002, NE2001.I. A New Model for the Galactic Distribution of Free Electrons and its Fluctuations, http://adsabs.harvard.edu/abs/2002astro.ph..7156C
de Bruyn, A. G. & Brentjens, M. A. 2005, Astronomy and Astrophysics, 441, 931
Eilek, J. A. 1989a, AJ, 98, 244
Eilek, J. A. 1989b, AJ, 98, 256
Enßlin, T. A. & Vogt, C. 2003, A&A, 401, 835
Fletcher, A. & Shukurov, A. 2007, in EAS Publications Series, Vol. 23, EAS Publications Series, ed. M.-A. Miville-Deschênes & F. Boulanger, 109–128
Frick, P., Sokoloff, D., Stepanov, R., & Beck, R. 2010, Monthly Notices of the Royal Astronomical Society, 401, L24
Frick, P., Sokoloff, D., Stepanov, R., & Beck, R. 2011, MNRAS, 557
Gaensler, B. M., Dickey, J. M., McClure-Griffiths, N. M., et al. 2001, ApJ, 549, 959
Gaensler, B. M., Landecker, T. L., Taylor, A. R., & POSSUM Collaboration. 2010, in Bulletin of the American Astronomical Society, Vol. 42, American Astronomical Society Meeting Abstracts #215, 515
Górski, K. M., Hivon, E., Banday, A. J., et al. 2005, ApJ, 622, 759
Haverkorn, M., Katgert, P., & de Bruyn, A. G. 2000, A&A, 356, L13
Heald, G., Braun, R., & Edmonds, R. 2009, Astronomy and Astrophysics, 503, 409
Jaffe, T. R., Leahy, J. P., Banday, A. J., et al. 2010, MNRAS, 401, 1013
Jansson, R., Farrar, G. R., Waelkens, A. H., & Enßlin, T. A. 2009, J. Cosmology Astropart. Phys., 7, 21
Junklewitz, H. & Enßlin, T. A. 2010, ArXiv e-prints
Kahniashvili, T. & Vachaspati, T. 2006, Phys. Rev. D, 73, 063507
Oppermann, N., Junklewitz, H., Robbers, G., & Enßlin, T. A. 2010, ArXiv e-prints
Pizzo, R. F., de Bruyn, A. G., Bernardi, G., & Brentjens, M. A. 2010, 1008.3530
Reich, W., Fürst, E., Reich, P., et al. 2004, in The Magnetized Interstellar Medium, ed. B. Uyaniker, W. Reich, & R. Wielebinski, 45–50
Rybicki, G. B. & Lightman, A. P. 2004, Radiative Processes in Astrophysics (Wiley-VCH)
Spangler, S. R. 1982, ApJ, 261, 310
Spangler, S. R. 1983, ApJ, 271, L49
Subramanian, K. 1999, Physical Review Letters, 83, 2957
Sun, X. H., Reich, W., Waelkens, A., & Enlin, T. A. 2008, Astronomy and Astrophysics, 477, 573
Tennekes, H. & Lumley, J. 1972, A First Course in Turbulence (The MIT Press)
Uyaniker, B., Fuerst, E., Reich, W., Reich, P., & Wielebinski, R. 1998, A&AS, 132, 401
Waelkens, A., Jaffe, T., Reinecke, M., Kitaura, F. S., & Enlin, T. A. 2009, Astronomy and Astrophysics, 495, 697
Waelkens, A. H., Schekochihin, A. A., & Enßlin, T. A. 2009, MNRAS, 398, 1970
Wolleben, M., Fletcher, A., Landecker, T. L., et al. 2010, 1011.0341
Wolleben, M., Landecker, T. L., Carretti, E., et al. 2009, in IAU Symposium, Vol. 259, IAU Symposium, 89–90

Appendix A: Derivation of the probability distribution for caustics

In this appendix we will derive the probability for measuring a spike with integrated intensity $\mathcal{F}$ given that the spike is due to a caustic (i.e. $B_3 = 0$) and a magnetic covariance matrix M. We will limit our discussion to the regime where the parameter u, defined in Sect. 2, is small so that Eq. (20) describes the integrated flux of the caustic.

In Sect. 2 we found that the integrated polarized intensity of a caustic is $\mathcal{F} = 4a_s\sqrt{\delta\phi}\,|B_\perp(0)|^2 / \sqrt{B_3'(0)a_1}$. We assume a Gaussian magnetic field distribution, $\mathcal{G}(B, M)$. The probability distribution of integrated intensities $\mathcal{F}$, given that $B_3 = 0$ and the magnetic correlation tensor is M is

$$P(\mathcal{F}|\text{caustic}, M) = \frac{P(\mathcal{F}, \text{caustic}|M)}{P(\text{caustic}|M)}. \tag{A.1}$$

The denominator, which is the probability that a caustic occurs in a Gaussian random magnetic field, is relatively straightforward to compute. We enforce that $B_3(0) = 0$ using a delta function and the probability is given by

$$P(\text{caustic}|M) = \int \mathcal{D}B\;\delta(B_3(0))\;\mathcal{G}(B, M). \tag{A.2}$$

where the integral is a path-integral over all possible realizations of the magnetic field. We then replace the delta function using the Fourier transform

$$P(\text{caustic}|M) = \frac{1}{\sqrt{|2\pi M|}}\int \mathcal{D}B \int d\eta\; e^{2\pi i\eta B_3}\; e^{-\frac{1}{2}B^\dagger M^{-1}B}. \tag{A.3}$$

We now replace ηB_3 with $\eta\delta_{i3}\boldsymbol{B}$ and after completing the square we have

$$P(\text{caustic}|M) = \frac{1}{|2\pi M|}\int \mathcal{D}B \int d\eta\;\exp\Big[-\frac{1}{2}\left(B - J^\dagger M\right)^\dagger M^{-1}\left(B - J^\dagger M\right) + \frac{1}{2}J^\dagger M J\Big]. \tag{A.4}$$

where $J^\dagger = 2\pi i\eta\delta_{iz}\delta(z)$. The $\boldsymbol{B}$ integral is the integral of a Gaussian function which results in a factor of $\sqrt{|2\pi M|}$. The η integral is also a Gaussian integral. After integration, the result is

$$P(\text{caustic}|M) = \sqrt{\frac{2\pi}{M_{33}(0)}}. \tag{A.5}$$

The calculation of the numerator of Eq. (A.1) is more involved. Again we start by enforcing our conditions using delta functions

$$P(\mathcal{F}, \text{caustic}|M) = \int \frac{\mathcal{D}B}{\sqrt{|2\pi M|}}\;\delta(B_3(0))\delta\Big(\mathcal{F} - \frac{a_s\sqrt{\delta\phi}B_\perp^2(0)}{\sqrt{B_3'(0)a_1}}\Big)\exp\Big[-\frac{1}{2}B^\dagger M^{-1}B\Big]. \tag{A.6}$$

Using Eq. (12) we rewrite the second delta function in terms of B_3

$$\delta\Big(\mathcal{F} - \frac{4a_s B_\perp^2(0)\sqrt{\delta\phi}}{\sqrt{B_3'(0)a_1}}\Big) = 4K\frac{B_\perp^4}{\mathcal{F}^3}\delta\Big(B_3'(0) - K\frac{B_\perp^4(0)}{\mathcal{F}^2}\Big). \tag{A.7}$$

where $K = 16a_s^2\delta\phi/a_1$.

Inserting this into Eq. (A.6), we now proceed with the calculation using the Fourier representation of the delta function:

$$\begin{aligned}&\int \frac{\mathcal{D}B}{\sqrt{|2\pi M|}}\;\delta(B_3(0))\;2K\frac{\delta\phi^2 B_\perp^4}{a_1^2\mathcal{F}^3}\;\delta\Big(B_3'(0) - K\frac{B_\perp^4(0)}{\mathcal{F}^2}\Big)\exp\Big[-\frac{1}{2}B^\dagger M^{-1}B\Big]\\ &= \frac{2K\delta\phi^2}{a_1^2\mathcal{F}^3}\int\frac{\mathcal{D}B}{\sqrt{|2\pi M|}}\int\frac{d\mu}{2\pi}\int\frac{d\eta}{2\pi}B_\perp^4(0)\exp\Big[-\frac{1}{2}B^\dagger M^{-1}B\Big]\exp[i\eta B_3(0)]\;\exp\Big[i\mu\Big(B_3'(0) - \frac{KB_\perp^4(0)}{\mathcal{F}^2}\Big)\Big]\end{aligned} \tag{A.8}$$

We further introduce two generalized fields $\mu' = \delta_{i3}\;\delta(x - x_0)\;\delta(y - y_0)\;\mu$ and $\eta' = \delta_{i3}\;\delta(x - x_0)\;\delta(y - y_0)\;\eta$ that permit us to work with the total magnetic field $B(z)$ rather than the LOS-component $B_3(z)$ in ((A.8)):

$$\frac{4K}{\mathcal{F}^3}\int\frac{\mathcal{D}B}{\sqrt{|2\pi M|}}\int\frac{d\mu}{2\pi}\int\frac{d\eta}{2\pi}\;B_\perp^4(0)\exp\Big[-i\mu\Big(\frac{KB_\perp^4(0)}{\mathcal{F}^2}\Big)\Big]\exp\Big[-\frac{1}{2}B^\dagger M^{-1}B + i(\eta' + \mu'\partial_3)^\dagger B\Big] \tag{A.9}$$

The functional integral over $\mathcal{D}B$ cannot be solved analytically because of the $B_\perp^4(z)$-term in the exponential. In general we will require diagrammatic perturbation theory in order to proceed.

If we restrict our attention to strong caustics we can proceed analytically. This is a reasonable restriction since it will be the strong caustics that are the most likely features to be observed. Note that a strong caustic can occur for two reasons: either if $B_\perp$ is large, or if B_3' is small. Strong caustics due to an exceptionally large sky plane magnetic field are not likely due to our assumption of Gaussian statistics, and therefore we concentrate on caustics with large $\mathcal{F}$ due to a slowly changing LOS magnetic field. For

those we can neglect the $B_\perp^4(z)/\mathcal{F}^4$-term and solve the remaining problem by introducing a generating functional J and repeatedly applying Gaussian integrations:

$$
\begin{aligned}
&\frac{4K}{\mathcal{F}^3}\int\frac{\mathcal{D}B}{\sqrt{|2\pi M|}}\int\frac{d\mu}{2\pi}\int\frac{d\eta}{2\pi}\,(B_1^2(0)+B_2^2(0))^2\exp\Big[-\frac{1}{2}B^\dagger M^{-1}B+i(\eta'+\mu'\partial_3)^\dagger B\Big]\\
&=\frac{4K}{\mathcal{F}^3}\int\frac{\mathcal{D}B}{\sqrt{|2\pi M|}}\int\frac{d\mu}{2\pi}\int\frac{d\eta}{2\pi}\Big[\Big(\frac{\delta}{\delta J_1(z)}\Big)^2+\Big(\frac{\delta}{\delta J_2(z)}\Big)^2\Big]^2\exp\Big[-\frac{1}{2}B^\dagger M^{-1}B+(i\eta'+i\mu'\partial_3+J)^\dagger B\Big]\Big\|_{J=0}\\
&=\frac{4K}{\mathcal{F}^3}\Big[\Big(\frac{\delta}{\delta J_1(z)}\Big)^2+\Big(\frac{\delta}{\delta J_2(z)}\Big)^2\Big]^2\int\frac{d\mu}{2\pi}\int\frac{d\eta}{2\pi}\exp\Big[\frac{1}{2}(i\eta'+i\mu'\partial_3+J)^\dagger M(i\eta'+i\mu'\partial_3+J)\Big]\Big\|_{J=0}\\
&=\frac{4K}{\mathcal{F}^3}\Big[\Big(\frac{\delta}{\delta J_1(z)}\Big)^2+\Big(\frac{\delta}{\delta J_2(z)}\Big)^2\Big]^2\int\frac{d\mu}{2\pi}\int\frac{d\eta}{2\pi}\exp\Big[-\frac{1}{2}\eta'^\dagger M\eta'-\frac{1}{2}(\mu'\partial_3)^\dagger M(\mu'\partial_3)+\frac{1}{2}J^\dagger MJ\\
&+\underbrace{\Big(-\frac{1}{2}(\eta'+J)^\dagger M(\mu'\partial_3)-\frac{1}{2}(\mu'\partial_3)^\dagger M(\eta'+J)\Big)}_{=0,\text{because } M_{33}(z,z') \text{ is at its maximum for } z,z'=0}+i\eta'^\dagger MJ\Big]\Big\|_{J=0}\\
&=\frac{4K}{\mathcal{F}^3}\frac{1}{\sqrt{2\pi|M_{33}''(0)|}}\Big[\Big(\frac{\delta}{\delta J_1(z)}\Big)^2+\Big(\frac{\delta}{\delta J_2(z)}\Big)^2\Big]^2\int\frac{d\eta}{2\pi}\exp\Big[-\frac{1}{2}\eta^2M_{33}(0)+i\eta\underbrace{\int dz'J_iM_{i3}(z',0)}_{=I}+\frac{1}{2}J^\dagger MJ\Big]\Big\|_{J=0}\\
&=\frac{4K}{\mathcal{F}^3}\frac{1}{\sqrt{2\pi|M_{33}(0)|}}\,\frac{1}{\sqrt{2\pi|M_{33}''(0)|}}\Big[\Big(\frac{\delta}{\delta J_1(z)}\Big)^2+\Big(\frac{\delta}{\delta J_2(z)}\Big)^2\Big]^2\exp\Big[\frac{1}{2}J^\dagger MJ-\frac{1}{2}\frac{I^2}{M_{33}(0)}\Big]\Big\|_{J=0}\\
&=\frac{4K}{\mathcal{F}^3}\frac{1}{\sqrt{2\pi|M_{33}(0)|}}\,\frac{1}{\sqrt{2\pi|M_{33}''(0)|}}\Big[3(M_{11}^2(0)+M_{22}^2(0))+M_{22}(0)M_{11}(0)+\frac{1}{M_{33}^2(0)}\underbrace{(M_{13}^4(0)+M_{23}^4(0)+2M_{23}^2(0)M_{13}^2(0))}_{=0}\Big]\\
&=\frac{28K}{\mathcal{F}^3}\frac{1}{\sqrt{2\pi|M_{33}(0)|}}\,\frac{1}{\sqrt{2\pi|M_{33}''(0)|}}M_N^2=\frac{28K}{\mathcal{F}^3}\frac{1}{\sqrt{2\pi|M_{33}(0)|}}\,\frac{1}{\sqrt{2\pi|M_{33}''(0)|}}\Big[\int\frac{dk^3}{(2\pi)^3}\,\hat{M}_N(k)\Big]^2\\
&=\frac{28K}{\mathcal{F}^3}\frac{1}{\sqrt{2\pi|M_{33}(0)|}}\,\frac{1}{\sqrt{2\pi|M_{33}''(0)|}}\Big[\int dk^3\,\frac{\epsilon_B(k)}{k^2}\Big]^2
\end{aligned}
\tag{A.10}
$$

In the last step we identified the covariance matrix M with the magnetic correlation tensor given by Eqs. (25) and (26). We used the property $M_{ij}(0)=M_N(0)\,\delta_{ij}$. Finally, from this result and Eq. (31), we conclude that in the bright caustic limit

$$
\begin{aligned}
P(\mathcal{F}|\text{caustic},M)&=\frac{P(\mathcal{F},\text{caustic}|M)}{P(\text{caustic}|M)}=\frac{448a_s^2\delta\phi^2}{\mathcal{F}^3a_1}\frac{M_N^2(0)}{\sqrt{2\pi|M_{33}''(0)|}}\\
&=\frac{448a_s^2\delta\phi^3}{\mathcal{F}^3a_1^2\sqrt{2\pi|M_{33}''(0)|}}\Big[\int dk^3\frac{\epsilon_B(k)}{k^2}\Big]^2=\frac{448a_s^2\delta\phi^3}{\mathcal{F}^3a_1^2\sqrt{2\pi}}\frac{\Big[\int dk^3\frac{\epsilon_B(k)}{k^2}\Big]^2}{\Big[\int dk^3\epsilon_B(k)\Big]^{1/2}}
\end{aligned}
\tag{A.11}
$$

Appendix B: Simulated Faraday spectral cube slices

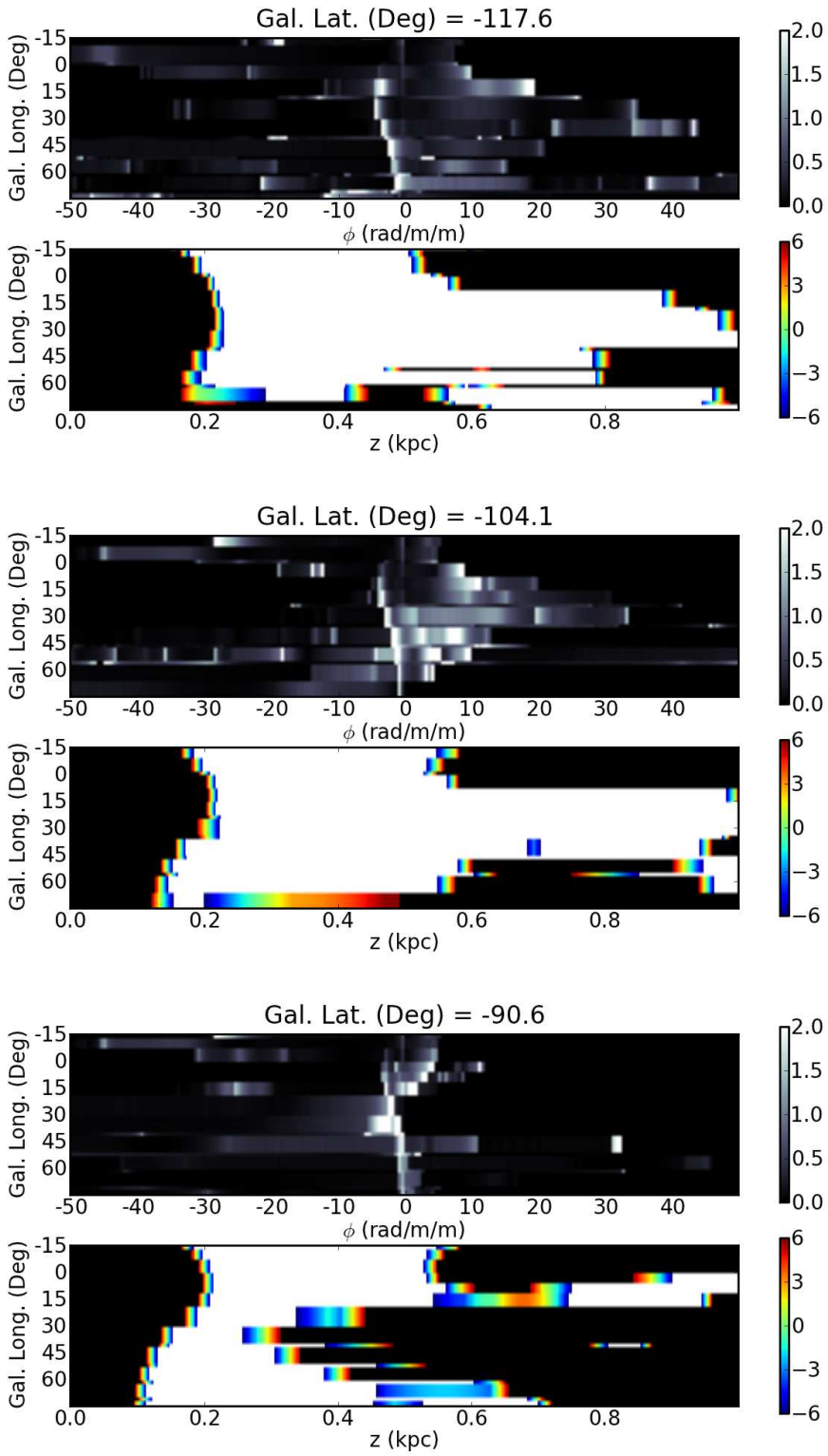

Fig. B.1. The first three slices of a Faraday spectrum cube of a Hammurabi simulation and the associated LOS magnetic field strength. Each pair shows a frame at a different Galactic latitude. Top: A grey scale image of polarized intensity (in arbitrary units) as a function of Faraday depth and Galactic longitude. Bottom: The LOS magnetic field strength as a function of LOS distance (in pc) and Galactic longitude. The scale has been compressed to highlight regions with opposite polarity. Black indicates positive magnetic field strengths and white negative. The colored area is where $B_3 \approx 0$ (appears as grey scale in text version).

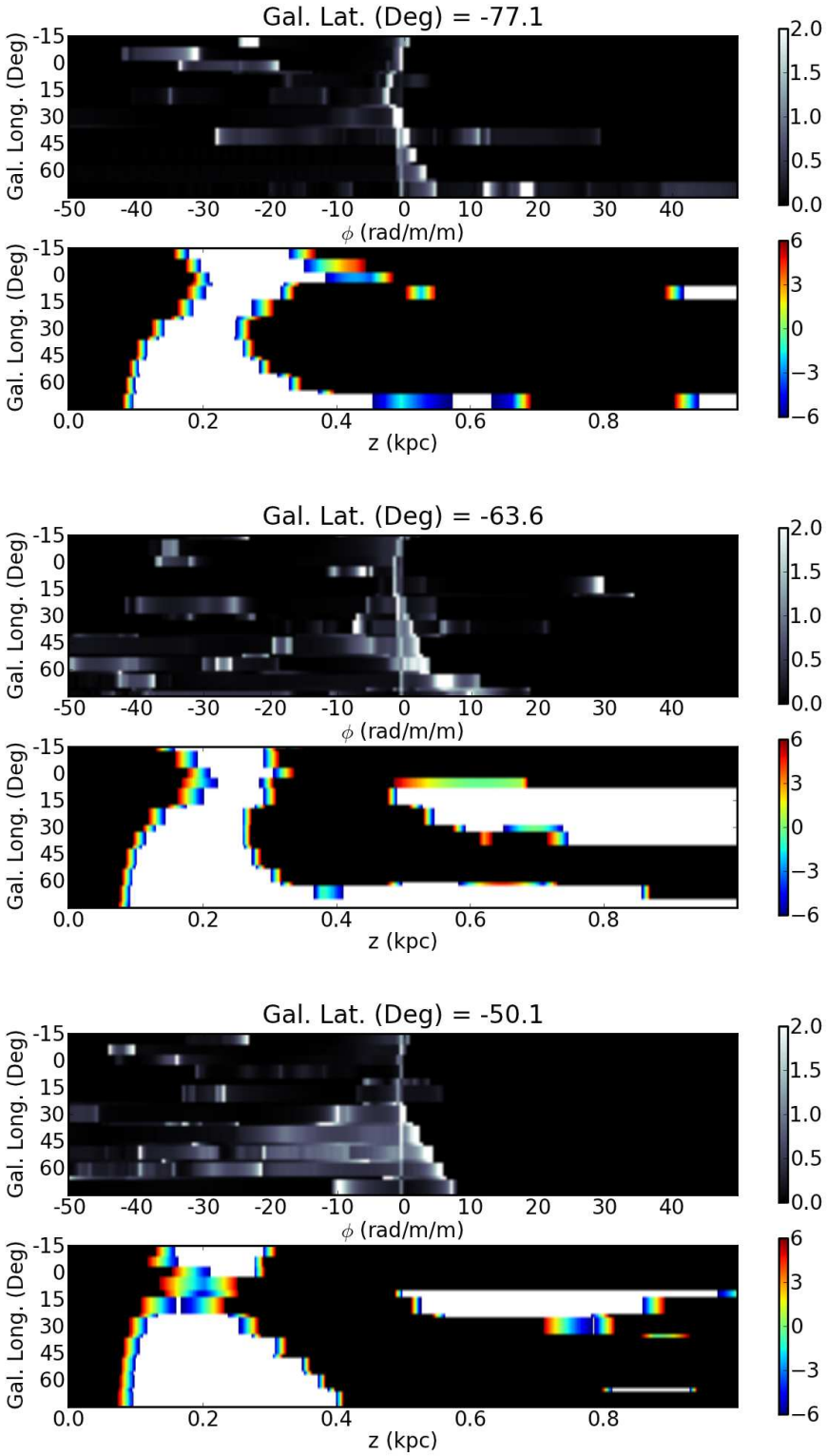

Fig. B.2. Three more slices of a Faraday spectrum cube of a Hammurabi simulation, following those in Fig. B.1.